Defining the Role of Matrix Compliance and Proteolysis in Three-Dimensional Cell Spreading and Remodeling

Daniel Dikovsky,*‡ Havazelet Bianco-Peled,†§ and Dror Seliktar*§
*Faculty of Biomedical Engineering, †Faculty of Chemical Engineering, ‡Inter-Departmental Program for Biotechnology, and §The Russell Berrie Nanotechnology Institute, Technion-Israel Institute of Technology, Technion City, Haifa 32000, Israel

ABSTRACT Recent studies have identified extracellular matrix (ECM) compliance as an influential factor in determining the fate of anchorage-dependent cells. We explore a method of examining the influence of ECM compliance on cell morphology and remodeling in three-dimensional culture. For this purpose, a biological ECM analog material was developed to pseudo-independently alter its biochemical and physical properties. A set of 18 material variants were prepared with shear modulus ranging from 10 to 700 Pa. Smooth muscle cells were encapsulated in these materials and time-lapse video microscopy was used to show a relationship between matrix modulus, proteolytic biodegradation, cell spreading, and cell compaction of the matrix. The proteolytic susceptibility of the matrix, the degree of matrix compaction, and the cell morphology were quantified for each of the material variants to correlate with the modulus data. The initial cell spreading into the hydrogel matrix was dependent on the proteolytic susceptibility of the materials, whereas the extent of cell compaction proved to be more correlated to the modulus of the material. Inhibition of matrix metalloproteinases profoundly affected initial cell spreading and remodeling even in the most compliant materials. We concluded that smooth muscle cells use proteolysis to form lamellipodia and tractional forces to contract and remodel their surrounding microenvironment. Matrix modulus can therefore be used to control the extent of cellular remodeling and compaction. This study further shows that the interconnection between matrix modulus and proteolytic resistance in the ECM may be partly uncoupled to provide insight into how cells interpret their physical three-dimensional microenvironment.

INTRODUCTION

The physical microenvironment of a cell is an important determinant of its behavior and can supersede biochemical signaling to dominate the inductive processes associated with tissue morphogenesis, homeostasis, and regeneration (1–4). It is surprising how little is known about biophysical stimulation in this regard, when compare with the vast body of knowledge surrounding biochemical agonists. To study biophysical induction requires differentiating between structural and biological milieus, which is not easy to do in the body's tissues. Many of the body's anchorage-dependent cells reside in a highly complex three-dimensional (3D) extracellular space crowded by biochemical and structural features that together regulate morphological behaviors and modulate phenotypic expression. The extracellular matrix (ECM) proteins themselves function as structural elements that simultaneously present many biological cell signaling motifs including adhesion ligands and proteolytic sites, two key elements in tissue remodeling (5–8). Reconstituted ECM proteins such as fibrin, collagen, and Matrigel have been used to mimic the natural 3D culture environment when investigating the influence of structural features on cell phenotype and cell migration ex vivo (9–12). Unfortunately, there has been limited success in precisely controlling the physical properties of reconstituted ECM proteins without either posing an impediment to the 3D culture of cells (13), or altering the ECM ligand density to control matrix stiffness (11,14).

Carefully designed experimental studies using two-dimensional (2D) culture systems have provided some insight into the structure/function relationship between the ECM mechanics and cell spreading, motility, proliferation, and differentiation (15–18). Monolayer cultures on adhesive and viscoelastic substrates whose ligand density and mechanics can be controlled independently are used to quantitatively couple bioactivity and substrate stiffness to cell spreading (19–21), cell phenotype (22), or cell motility (23). Enhanced biomaterials can be used to provide a more physiologically relevant presentation of biochemical signals without compromising the ability to exactingly control the matrix compliance (24). However, a 2D monolayer culture system can never emulate the complexities of the 3D tissue microenvironment, and will always represent a suboptimal milieu for studying physiological ECM interactions with connective tissue cells (2,7,25,26). Indeed, many researchers are recognizing the limitations of monolayer cell cultures (27), but are invariably faced with no better alternatives when embracing the 3D context of cell culture. The inability to precisely control the physical properties of the ECM independent of its biochemistry in 3D is one of the reasons for the continued use of 2D system for this type of investigation.

We developed a biological ECM analog material that can pseudo-independently alter its biochemistry and physical

Submitted February 5, 2007, and accepted for publication November 30, 2007.

Address reprint requests to Dr. Dror Seliktar, The Faculty of Biomedical Engineering, Technion-Israel Institute of Technology, Technion City, Haifa 32000, Israel. Tel.: 972-4-829-4805 Fax: 972-4-829-4599; E-mail: dror@bm.technion.ac.il

Editor: Gaudenz Danuser.

0006-3495/08/04/2914/12 $2.00

doi: 10.1529/biophysj.107.105841

properties to begin to investigate physical induction of mammalian cells in 3D (28,29). The basis of the 3D matrix is fibrinogen, a biologically active template for cell culture, which was conjugated with an inert polymer, poly(ethylene glycol) (PEG), to create a protein–polymer mosaic (30). The synthetic polymer in the system precisely interacts with the protein according to its relative size and quantity of the conjugation sites to alter both the physical and biochemical properties of the cell culture environment (31). Using cultures of encapsulated smooth muscle cells (SMCs) we were able to show how distinct changes to the mechanics or proteolytic resistance of the ECM analog have profound influence on 3D cell morphology within the matrix and subsequent matrix remolding.

MATERIALS AND METHODS

Fibrinogen PEGylation and hydrogel preparation

PEG-diacrylate (PEG-DA) was prepared as described elsewhere (32). Briefly, three species of PEG-OH: linear PEG with an average molecular weight of 10 kDa, 20 kDa (Aldrich, Sleeze, Germany), and 4-arm PEG with an average molecular weight of 20 kDa (Nektar, Huntsville, AL) were reacted with acryloyl chloride (Merck, Darstadt, Germany) at a molar ratio of 1.75:1 relative to −OH groups in dichloromethane and triethylamine (Fluka, Buchs, Switzerland). The final product was precipitated in ice-cold diethyl ether, dried under vacuum, and the end-group conversion of the product was confirmed by H^1NMR to be 99% (data not shown). Conjugation of the linear PEG-DA (10-kDa and 20-kDa) to cysteines on denatured bovine fibrinogen was done as described elsewhere (31). The fibrinogen concentration in the product was determined using the BCA standard assay (Pierce Biotechnology, Rockford, IL) and the degree of PEG substitution was calculated according to published protocols (31). The hydrogel was formed by photopolymerization of the PEGylated fibrinogen (PF) solution, after 5 min exposure to ultraviolet (UV) light (365 nm, 4–5 mW/cm^2) in the presence of 0.1% W/V Irgacure 2959 photoinitiator (Ciba Specialty Chemicals, Tarrytown, NY).

Rheological characterization

PF precursor solution (200 μL) containing photoinitiator was placed in a strain-rate controlled shear rheometer with parallel-plate geometry (ARES, TA Instruments, New Castle, DE). Three oscillatory tests were done: time-sweep, strain-sweep, and frequency-sweep. The time-sweep was done for 5 min with a 5% sinusoidal strain (1 rad/sec) to monitor the in situ gelation of the PF solutions during the photopolymerization reaction. The strain-sweep test was done with a strain range between 1% to 100% at a frequency of 1 rad/sec. The frequency-sweep test was done with a frequency range of 0.1–100 rad/s up to 5% maximum strain. At least six samples of PF materials from at least three different batches were tested. All rheometry testing was done at 37°C with a 30-s preconditioning cycle. The PF solutions were polymerized in the rheometer by exposing the samples to UV light (365 nm, ~20 mW/cm^2) while the storage and loss modulus values (G', G'') were continuously recorded with RSIs Orchestrator software. The reported shear modulus was taken as the real part of the complex shear modulus $G^* = G' + iG''$ at the conclusion of the test based on the rationale that the loss modulus was negligible in comparison the storage modulus of each sample.

Swelling characterization

Cylindrical specimens were prepared by polymerizing PF precursor solution in silicone molds. The specimens were submerged in 150 mM phosphate buffered saline (PBS) containing 0.1% sodium azide at 37°C for 24 hr. The specimen's final swollen weight ($W_{swollen}$) was recorded before being lyophilized overnight and weighted in its dry state (W_{dry}). The water content at equilibrium was calculated from this data as follows: $(W_{swollen} - W_{dry})/W_{swollen}$.

Enzyme degradation

Cylindrical PF specimens were prepared and labeled with succinimidyl acridine-9-carboxylate (SAC) (Sigma-Aldrich, St. Louis, MO) as described elsewhere (33). SAC is an amine-reactive blue-fluorescent probe that selectively binds the fibrinogen backbone of the hydrogel specimen. After removal of unreacted SAC by sequential washes, the degradation experiment was done by measuring release of fluorescently-labeled fibrinogen (ex@364 nm, em@460 nm) from the enzymatically dissolved hydrogel fraction. The rate of degradation was characterized in 0.01 mg/ml trypsin solution (Sigma-Aldrich) in 150 mM PBS (pH 7.4) containing 0.1% sodium azide. Negative controls contained stained specimens without enzyme or unstained specimens with enzyme solution.

SMC constructs

Smooth muscle cells (SMCs) were harvested from bovine aorta and cultured according to standard protocols. The SMCs were maintained for up to seven passages in Dulbecco modified Eagle medium (DMEM) (Gibco, UK) containing 10% fetal bovine serum (FBS) (Biological Industries, Israel), 1% penicillin-streptomycin (Biological Industries), and 1% L-glutamine (Gibco). The SMCs were dispersed in 400 μL of PF precursor solution (1×10^6 cells/ml) and exposed to UV light (365 nm at 4–5 mW/cm^2) in the presence of photoinitiator. Viability testing was done on the encapsulated SMCs in the PF hydrogels after 2 h and 3 days in culture. The cells were first removed from the constructs by dissolving the fibrinogen backbone in a 1 mg/ml solution of collagenase type IA (Sigma-Aldrich) for 2 h followed by 5 min centrifugation (1000 rpm). Finally, the cells were dispersed in trypan blue solution and counted in a hemocytometer. The live and dead cell numbers were recorded and normalized to a control suspension of collagenase-treated cells that were not encapsulated.

SMC morphology and remodeling

Cellular morphology was monitored by phase contrast microscopy using a time-lapse system with temperature, humidity, and CO_2 controlled environment situated on a Nikon TE2000 microscope equipped with an x-y-z motorized stage controller and a digital CCD camera. Time-lapse experiments were carried out for up to 3 days in 48-well plates containing the PF constructs in ample culture medium. Multiple locations within each construct were imaged in 5 min intervals for the duration of the experiment. The migration and local contraction by SMCs within PF materials was quantified by co-encapsulating 2-μm latex beads (5 million beads per milliliter) together with the cells into the transparent hydrogels and imaging the samples in 5 min increments (time-lapse). The images were stacked together; contrast enhancement and alignment were done using ImageJ software with the StackReg plugin (34). The beads were tracked in each frame and the incremental bead displacement vectors of individual beads surrounding the cells were measured at various locations within each construct. For presentation purposes, several beads of interest were marked with color using the Manual Tracking feature of ImageJ software. Discrete changes to cell morphology were monitored by labeling the cytoskeleton of cells within the PF constructs. F-actin was fluorescently labeled with Phalloidin (Sigma-Aldrich) and cells were counterstained with Hoechst 33342 (Sigma-Aldrich). The fluorescently-labeled cells were visualized and imaged on a Nikon TE2000 microscope equipped with a Prosilica CV640 digital CCD camera (Prosilica, BC, Canada). Macroscopic contraction of the cell-seeded constructs was documented by measuring the construct diameter after 3 and 7 days in culture using a Nikon S100 microscope. The diameter measurements were normalized with the swollen construct diameter. Negative controls consisted of acellular PF hydrogels.

Protease characterization and inhibition

Western blotting for matrix metalloproteinases (MMPs) was done with antibodies from the MMP/TIMP antibody sampler kit I (Calbiochem, Darstadt, Germany). SMC constructs were prepared as described previously and cultured for 3 days. Each construct was homogenized and sonicated for 1 min in 400 μL of lysis buffer, centrifuged at 14,000 rpm for 2 min, and loaded onto individual lanes of a 10% polyacrylamide gel for SDS-PAGE analysis. Control samples included DMEM, PF solution (10 kDa), and lysis buffer. The separated proteins were transferred onto a nitrocellulose membrane, blocked, and labeled with primary antibodies against MMP-2, MMP-3, and MMP-9 (1 μg/mL solution). A mouse HRP-conjugated secondary antibody (Sigma) was diluted 1:1000 and incubated with the membrane before ECL detection (Santa Cruz Biotechnology, Santa Cruz, CA) and imaging using a Fujifilm LAS-3000 gel imaging system (Fujifilm Corporation, Japan). MMP inhibition was done using soluble inhibitors in DMSO added to the culture medium of the constructs according to manufacturer's instructions. The final DMSO concentration in the medium was below 2% (V/V). The following concentrations of inhibitor were tested: 0.6 mM MMP 2/9 Inhibitor I, 0.3 mM MMP 3 Inhibitor II, and 0.1 mM MMP 8 Inhibitor I. Control samples included constructs without inhibitor, constructs with 2% (V/V) DMSO, and SMCs cultured on 2D tissue culture plastic (TCP) in the presence of 0.6 mM MMP 2/9 inhibitor.

Immunohistochemistry

SMC-seeded constructs were prepared as described previously and cultured for 3 days. The constructs were frozen and sliced into 7–30 μm sections using a cryostat. Immunofluorescent labeling of collagen type I in the sections was accomplished using an anti-type I collagen primary antibody (Chemicon, Temecula, CA). A Cy3-conjugated secondary antibody (Chemicon) was used to identify type I collagen in fluorescent red. A Hoechst 33342 fluorescent blue counter-stain (Sigma-Aldrich) was used to label the cell nuclei in each section. The fluorescently-labeled cells were visualized and imaged using a Nikon TE2000 microscope and a digital CCD camera.

Statistical analysis

Statistical analysis was done using the Microsoft Excel statistical analysis software. Data from at least two independent experiments were analyzed for each variable. Comparisons between multiple treatments were made with analysis of variance (ANOVA) whereas ad-hoc comparisons between two treatments were made using a two-tail Student's t-test with $p < 0.05$ considered statistically significant.

RESULTS AND DISCUSSION

The hypothesis of this research asserted that during the initial phases of cellular spreading within an amorphous hydrogel, the dense macromolecular matrix obstructs the cell's lamellipodia and limits their spindled morphology. It is thought that cells cannot overcome the mechanical barrier of the matrix, other than by enzymatically breaking down their ECM microenvironment and then facilitating cellular extension of lamellipodia (i.e., tunneling) (35,36). Once spindled, the cells can exert tractional forces on the matrix and physically remodel their microenvironment. The proteolytic resistance of the ECM should therefore be a key factor in enabling enzyme-producing cells to manipulate their microenvironment to the extent that they can properly express remodeling morphology. On the other hand, it is the ECM modulus that, in theory, should be the dominant factor in regulating the remodeling events that follow the initial cell spreading. To begin to appreciate the respective roles of proteolysis and matrix stiffness in 3D cellular behavior within amorphous hydrogels, we constructed a set of biomimetic materials capable of supporting 3D cell remodeling and also being precisely tunable both in terms of matrix modulus and proteolytic resistance. This ECM analog was used to encapsulate cells and to measure hallmarks of cellular remodeling as both modulus and proteolytic resistance of the matrix were changed as part of the experimental design.

Matrix for 3D culture

Making a matrix for cell encapsulation that supports cell remodeling requires both proteolytic biodegradability and biological activity (e.g., cell adhesion sites). A malleable polymer constituent can be used to exactly control the physicochemical properties of the material. Accordingly, a 3D matrix was made by conjugating PEG polymer chains to cysteines on denatured fibrinogen and then cross-linking the PEGylated fibrinogen precursor using a photo-polymerization reaction (Fig. 1). During the free-radical reaction, free double bonds on the pendant PEG-acrylate chains are rapidly cross-linked to form an amorphous, macromolecular network of PEGylated fibrinogen characterized by a nanoscale microarchitecture and mesh size typical of most PEG-based hydrogels (31,35,37,38). The PF hydrogel presented a markedly

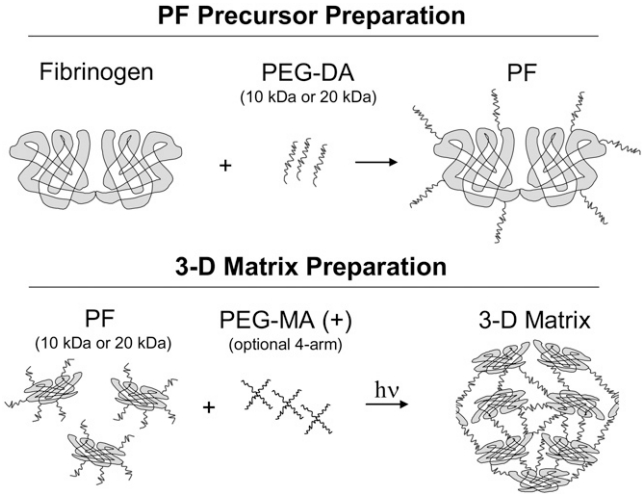

FIGURE 1 Schematic illustration of the biomimetic materials used for controlling matrix modulus and proteolytic resistance when studying 3D cellular remodeling. Preparation of the material precursor involved conjugating poly(ethylene glycol) (PEG) molecules (10- and 20-kDa) to denatured fibrinogen to form a protein–polymer macromer. The PF macromers were cross-linked by a light activated free-radical reaction (photopolymerization) with or without additional 4-arm star PEG-multiacrylate cross-linker (denoted by +) to form the 3D matrix. The fibrinogen backbone ensures biodegradability and biological activity whereas the PEG provides control of the physicochemical properties.

different microenvironment to encapsulated cells when compare with microfibrillar materials such as reconstituted ECM proteins (e.g., collagen, fibrin, Matrigel) (35). Beyond the cross-linking attributed to photopolymerization, it is unlikely that other protein-protein interactions (i.e., fibrillogenesis) actively participated in the PF hydrogel formation during the 5 min reaction. Although it is difficult to quantify precisely the pore diameter of amorphous PEG-based materials (35), previous approximations by our group yielded a theoretical mesh size on the order of tens of nanometers (31). The molecular weight (MW) of the PEG diacrylate (PEG-DA) chains (10- or 20-kDa) and the addition of a 1% (w/v) 4-arm star PEG multiacrylate (PEG-MA) cross-linker (denoted by +) represented two independent variables to control the physicochemical properties of the matrix in the experimental design. The protein concentration in the precursor (3–9 mg/ml) was used as an additional independent variable in the experimental design to provide further control over the relative bioactivity and physical properties of the matrix. There were a total of 18 different material variants that were created with the various combinations of constituents (Table 1). The water content of these materials showed that they were all highly swollen in PBS, containing between 97–99% water at equilibrium (Table 1). Increasing the concentration of the PF precursor and/or adding PEG-MA cross-linker had marginal effects on the water content of the materials. Alterations to the PEG/protein composition impacted the theoretical mesh size (31); however, these values remained in the nanometer scale and were far smaller than the characteristic length of cellular lamellipodia.

A detailed characterization of the mechanical properties of the PF hydrogel materials was performed to rank the compliance of the polymeric matrix relative to its composition. The in situ rheological characterization of the PF polymerization reaction showed rapid network formation from liquid precursor and a substantial impact of the PEG constituent on the shear modulus (G') of the polymerized matrix at any given protein concentration (Fig. 2 *A*). The viscoelastic properties of the PF materials (including thrombin-polymerized fibrin hydrogels and PEG-only hydrogels for comparison) were measured by rheological dynamic frequency-sweep and strain-sweep tests. The PF materials proved to be similar to PEG controls, in that their frequency and strain dependence of the storage and loss modulus was negligible, irrespective of their composition (Fig. 2 *B* and *C*). The thrombin-polymerized fibrin hydrogels, in contrast, exhibited nonlinear shear and loss moduli in the frequency and strain sweep tests. The shear modulus of the PF hydrogels increased proportionally with the number of PEG functional end-groups available during the photopolymerization reaction, irrespective of their source (e.g., additional PEG-MA cross-linker or increased precursor concentration). Interestingly, the increase in PEG chain length (MW) at any given precursor concentration caused the modulus of the matrix to increase even though no additional functional groups were added as a consequence of this change. Fig. 2 *B* summarizes the shear modulus of the materials as a function of the precursor concentration to show the capability of adjusting matrix compliance independently of biological content. It is worth noting that the biological content in this regard is proportional to the protein concentration; however, the relative relationship between the PEG chains and the protein backbone may also alter the protein's bioactivity and proteolytic susceptibility (39). The interconnection between proteolytic responsiveness of the PEGylated fibrinogen network and its mechanical properties was characterized before investigating the role of modulus in cellular remodeling of the hydrogels.

The assumption that a link exists between the proteolysis and composition of the PF materials was based on our current understanding of how PEGylation of therapeutic proteins affects their enzymatic cleavage (40). The proteolytic degradation of PEGylated proteins is altered by the steric hindrances imposed by the pendant PEG chains. Moreover, physical obstructions imposed by the dense hydrogel network may also reduce the mobility of certain proteases in the PEGylated fibrinogen hydrogel. To better understand the relationship between composition and enzymatic hydrogel degradation, the proteolytic susceptibility of the PF materials was characterized in 0.01 mg/ml trypsin solution using fluorescently labeled fibrinogen and time-resolved spectrofluorometry (Fig. 3). The degradation profiles showed that all three variables in the experimental design (i.e., protein precursor concentration, the relative amount of PEG, and the PEG MW) affected the degradation kinetics to some extent when using half-life (t_{50}) as a characteristic measure of degradation rate. In the interpretation of the degradation results,

TABLE 1 Water content in PF hydrogels (in %)

Precursor protein content (mg/ml)	PF10	PF10 (+)	PF20	PF20 (+)
8	98.13 ± 0.12	97.81 ± 0.11	–	–
7	98.20 ± 0.22	97.91 ± 0.31	98.24 ± 0.11	98.12 ± 0.05
6	98.52 ± 0.16	98.28 ± 0.15	98.56 ± 0.17	98.29 ± 0.08
5	98.82 ± 0.14	98.37 ± 0.24	98.79 ± 0.10	98.25 ± 0.15
4	–	–	99.00 ± 0.09	98.55 ± 0.11
3	–	–	–	98.69 ± 0.19

Summary of the water content values, $(W_{swollen} - W_{dry})/W_{swollen}$, for a set of four different PF formulations with 3–8 mg/ml protein concentration (proportional to the total precursor concentration).

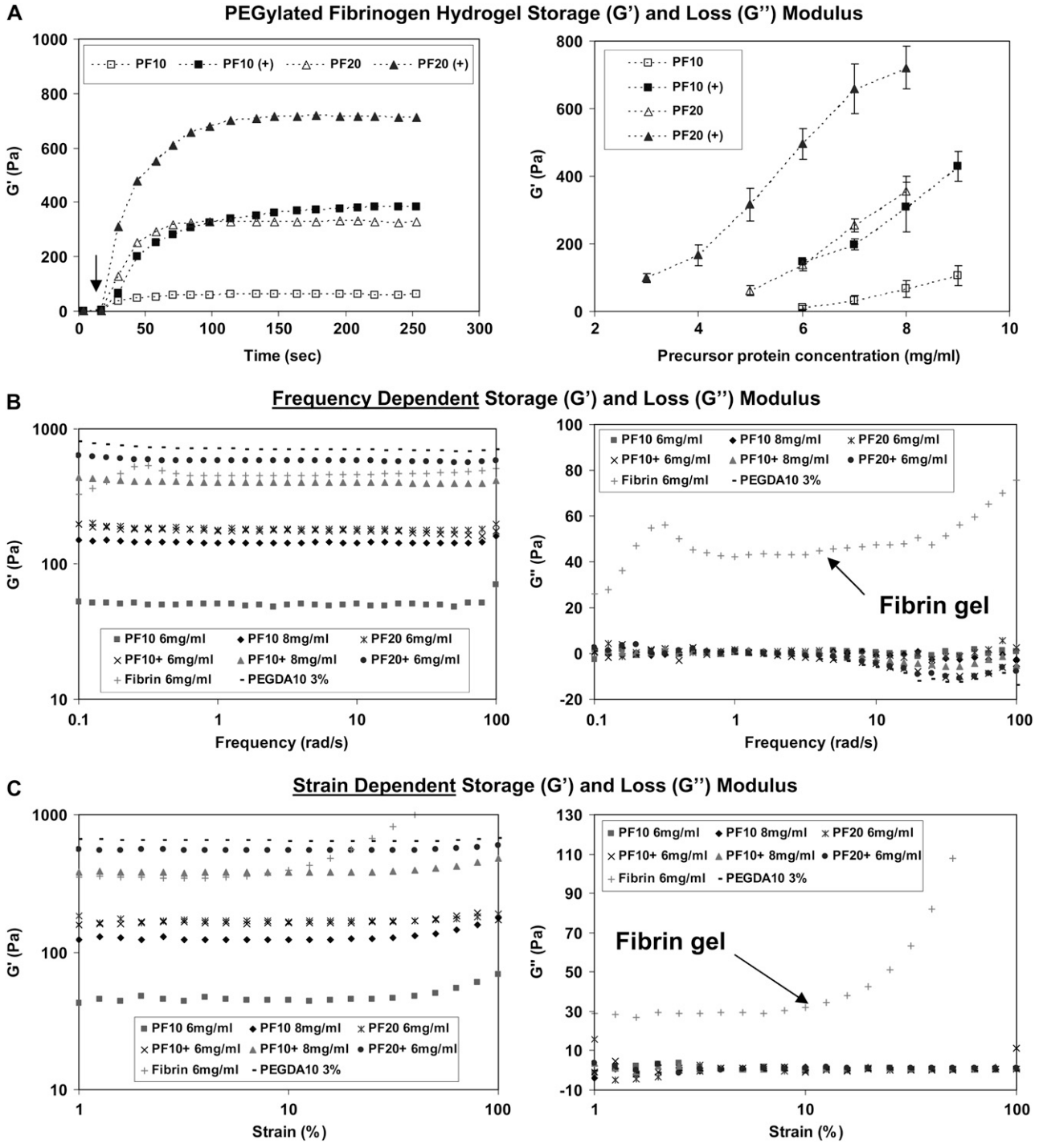

FIGURE 2 The modulus of the biomimetic PF matrix can be precisely controlled through its composition. (*A*) On the left, the shear modulus profiles (G′) during photopolymerization (30 s into the time-sweep) illustrates the rapid liquid-to-solid transition of the materials. The arrow indicates the location on the graph where G′ and G″ intersect (G″ not shown). The time-sweep curves correspond to four PF materials (8 mg/ml) made with different precursor formulations. The plateau shear modulus value (G′) was used to describe the stiffness of each material. On the right, a comparative plot of shear modulus as a function of precursor protein concentration for the four different formulations illustrates the composition dependence of the matrix mechanics. The shear modulus value (G′) is represented as the mean ± SD of at least three different batches of the PF material in each data point. (*B*) Frequency-dependent storage (G′) and loss (G″) modulus from oscillatory frequency-sweep rheological testing of PF, PEG-DA and fibrin only hydrogels. (*C*) Strain-dependent storage (G′) and loss (G″) modulus from strain sweep rheological testing of PF, PEG-DA and fibrin only hydrogels.

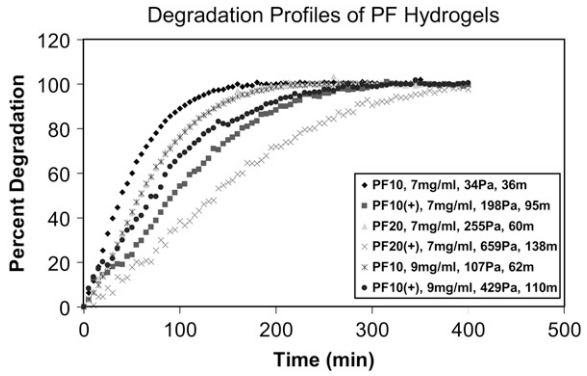

FIGURE 3 The proteolytic sensitivity of the PF matrix is composition dependent. Degradation profiles of the various PF hydrogels were recorded by quantifying the release kinetics of fluorescently labeled fibrinogen from the intact matrix over the course of an 8-h incubation in trypsin solution. The graph associates matrix degradation kinetics (percent degradation profile) with the three independent variables used to control the physicochemical properties of the PF matrix in the experimental design: PEG MW (10- and 20-kDa), precursor protein concentration (7 and 9 mg/ml) and additional PEG-multiacrylate cross-linker (+). Each material is represented in the legend by its composition, degradation half-life (t_{50} in min) and shear modulus (G′ in Pa).

half-life was merely used as a measure of proteolytic susceptibility of the PF materials but not intended to represent the physiological rate of cell-mediated biodegradation. We can assume that proteolytic susceptibility of the PF hydrogels is modulated by the interaction between the protease and the PEGylated protein backbone of the material, and therefore, degradation rate should be influenced by the fibrinogen concentration, cross-linking density and PEG MW. Furthermore, we can roughly appraise the material's proteolytic susceptibility to cell-secreted matrix-degrading enzymes a priori based on the observations from the experimental degradation data.

3D cell morphology

It is particularly important to interpret the cell remodeling behavior in each material with respect to its composition, modulus and resistance to proteolysis. With all 18 material variants characterized in this regard, cells were encapsulated and cultured for several days. Initially the SMCs were homogeneously suspended in the PF precursor solution and encapsulated during the photopolymerization. The SMCs immediately began to invade the dense matrix through cellular lamellipodia that protruded to all directions. Time-lapse video microscopy was used to capture these events occurring in materials whose stiffness was increased, to illustrate the relationship between the modulus and the dynamic processes that lead to the final morphology of the cells after 30 h in culture (Supplementary Material, Video 1). SMC morphology was highly spindled in the most compliant materials and completely rounded in the stiffest materials after 30 h. For comparison, a qualitative spindled index was used to classify the length and morphology of the typical lamellipodia extensions of the SMCs within the hydrogel after 30 h in all 18 materials tested as part of the experimental design. The spindled index was ranked based on the appearance of the cellular lamellipodia: 4, highly spindled with regular lamellipodia (Fig. 4 *A*); 3, spindled with frayed lamellipodia (Fig. 4 *B*); 2, nonspindled with frayed lamellipodia (Fig. 4 *C*); 1, rounded with minor lamellipodia (Fig. 4 *D*); 0, completely rounded with no lamellipodia (not shown). The spindled index reflected the ability of the cells to remodel their microenvironment but was very different from the quantitative shape indices typically used in 2D studies. Other methods used to more accurately calculate cell spreading in 2D culture systems were difficult to implement in the 3D culture system (41). Despite the rounded morphologies in the stiffest materials, cell viability in these cultures was not compromised as shown by quantitative assessment after 2 h and 3 days. Table 2 summarizes the viability data to show that the fraction of viable SMCs in all materials 2 h after photo-polymerization was $>73\%$ and did not decrease after 3 days in culture. There was no significant difference in the fraction of viable cells in any of the four variations of materials at any given protein concentration and time-point ($n \geq 6$, $p > 0.05$).

Short-term cellular remodeling

The cellular activity occurring in each material during the first 30 h of culture was observed by microscopic time-lapse video sequences (Supplementary Material, Video 1). During this initial stage of remodeling, the cells exhibited spreading, motility, contraction, and proliferation within the dense hydrogel matrix; the extent of which was highly dependent on the composition of the material. It is not clear which factor, either modulus or proteolytic susceptibility, had a more profound effect on these behaviors. In the video data, the compliant materials clearly favor more spindled morphology, whereas the rounded cell morphology was apparent in the stiffer materials. However, it was difficult to draw definitive conclusions about the effects of matrix stiffness on cell behavior in 3D without accounting in some way for the impact of proteolytic susceptibility of the 3D matrix. This is because in the PF hydrogel system, as in the natural ECM, the physical properties of the matrix and the proteolytic susceptibility will never be truly independent. Indeed, there was a reasonable correlation ($R^2 = 0.77$) between the shear modulus and the degradation t_{50} when comparing all PF variants (Fig. 5 *A*). This correlation confirms that there was no simple method of increasing the modulus without also increasing the degradation time of the hydrogel.

To appreciate the overall relationship between modulus, proteolysis and cell spreading (as measured by the spindled index) in all 18 material variants, a set of two correlation charts were prepared (Fig. 5 *B* and *C*). Fig. 5 *B* illustrates that the spindled index was higher in the lower range of the

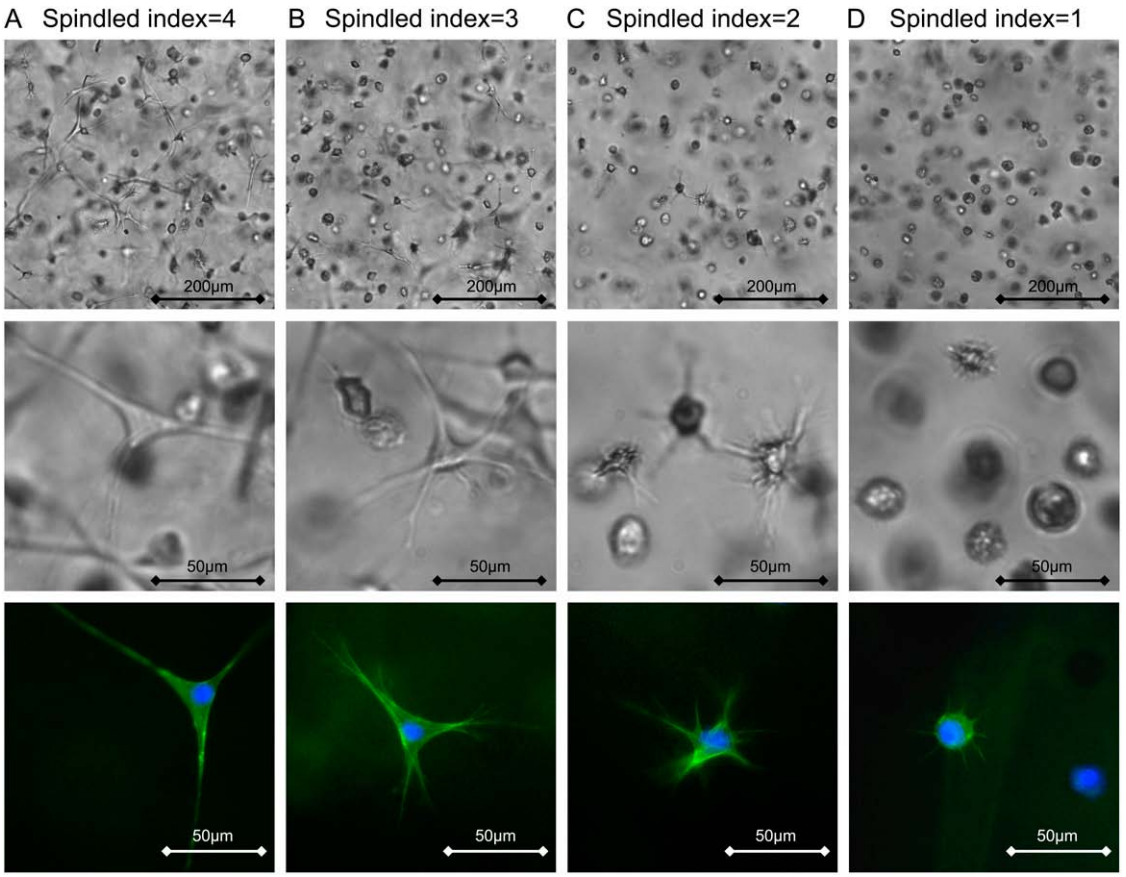

FIGURE 4 Encapsulated smooth muscle cells (SMCs) in PF hydrogels express different morphologies depending on the material composition. SMC morphology after 24 h in 3D culture was visualized by phase contrast microscopy (*top* and *middle rows*) and f-actin was visualized by fluorescent microscopy (*bottom row*). A differential spindled index scale (0-4) was used to characterize the typical SMC morphologies observed in the various materials. The spindled index was ranked as follows: 4, highly spindled with regular lamellipodia (*A*); 3, spindled with frayed lamellipodia (*B*); 2, nonspindled with frayed lamellipodia (*C*); 1, rounded with minor lamellipodia (*D*); 0, completely rounded (not shown). The materials shown include the following variations: PF10 having a modulus of 11.6 ± 6 Pa (*A*); PF10 having a modulus of 67 ± 25 Pa (*B*); PF10+ having a modulus of 147 ± 6 Pa (*C*); PF20+ having a modulus of 497 ± 45 Pa (*D*).

modulus scale as indicated by the more spindled morphology in materials having a 0–100 Pa modulus, compare with the higher modulus range where cells were less likely to form long lamellipodia into the matrix after 30 hr. Fig. 5 *C* showed a similar trend, whereby cells were more likely to become spindled in the faster degrading materials. Careful inspection of the materials in the lower modulus range showed that spindled index was less correlated with proteolytic half-life in this subset, even though they exhibited better correlation between modulus and spreading. This result suggests that in these materials, the effect of modulus on 3D cellular morphology was less dependent on the proteolytic susceptibility of the matrix, but still depended on proteolysis. Nevertheless, the limited resolving power and subjectivity of the 5-point spindled index scale makes it difficult to definitively conclude that modulus supersedes proteolytic sensitivity in regulating the 3D cell spreading in this range.

TABLE 2 Viability of SMCs in PF hydrogels (in %)

Material	2 h	3 days
PF10	73.8 ± 6.3	76.9 ± 7.5
PF10 (+)	75.4 ± 12.1	75.5 ± 8.9
PF20	76.3 ± 4.0	82.0 ± 5.4
PF20 (+)	73.7 ± 8.1	84.6 ± 6.0

Percent viable cells in PF hydrogels after 2 h and after 3 days in culture.

Long-term cellular remodeling

After additional culture time (up to 7 days) the encapsulated SMCs continue to form more lamellipodia and eventually become spindled in most of the PF hydrogels, with exception of the stiffest materials (PF20+, 7 mg/ml). Knowing the hydrogel stiffness does not change in the absence of proteases during the first week, the additional cell spreading is attributed mainly to the proteolytic dismantling of the impeding PF matrix that encapsulated the cells initially. In this regard, it is not evident to what extent the PF matrix needs to be locally

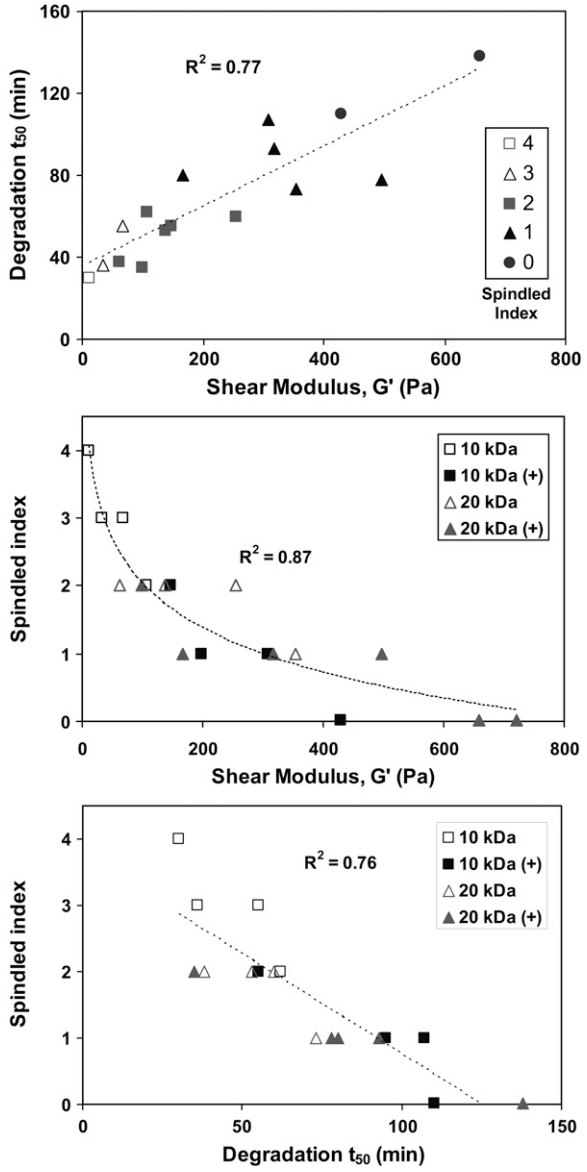

FIGURE 5 Correlation charts representing interdependence between modulus, proteolysis, and spindled index. (*Top*) The correlation between the shear modulus (G′) and degradation half-life (t_{50}) of the material is shown with a curve-fit linear regression ($R^2 = 0.71$). (*Middle*) The correlation between the shear modulus (G′) of the material and the SMCs spindled index is shown with a curve-fit logarithmic regression ($R^2 = 0.87$). (*Bottom*) The correlation between the degradation half-life (t_{50}) of the material and the SMCs spindled index is shown with a curve-fit linear regression ($R^2 = 0.76$).

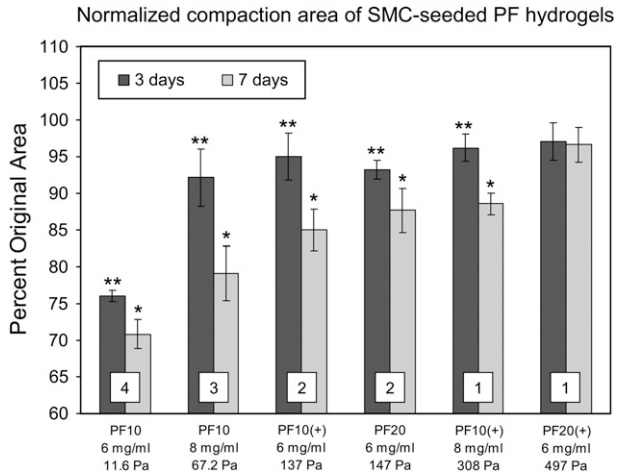

FIGURE 6 The material composition and matrix stiffness influence macroscopic compaction of SMC-seeded PF hydrogel constructs. The compaction data is taken from the diameter measurements of the constructs after 3 and 7 days in culture and normalized to acellular controls. The extent of compaction in each material is dependent on its composition and can be linked to the matrix modulus (reported in Pa) and cells initial spindled index at 30 h (shown for each treatment as a numeric insert). *Statistically significant difference between day 3 and day 7 ($p < 0.05$, $n \geq 6$). **Statistically significant difference between day 3 and no compaction (100%) ($p < 0.05$, $n \geq 6$).

degraded before cells may penetrate it with their lamellipodia. It was interesting to note that at the macroscopic scale, the cellular events (including cell spreading) were manifest as global changes to the tissue morphology based on observations that the cells physically compact the construct. The normalized diameter of the SMC-seeded constructs after compaction reflects the ease (or difficulty) in which cells can remodel the matrix at this macroscopic scale (Fig. 6). The material stiffness affected this compaction as is apparent in a quantitative comparison between compaction data, culture time and shear modulus values (G′) for each specified material. After 3 days, only the most compliant material shown (PF 10, 6 mg/ml) was compacted by more than 10%; whereas after 7 days, only the stiffest material shown (PF 20+, 6 mg/ml) was not compacted to this extent. Although the modulus was poorly correlated to compaction at day 3 ($R^2 = 0.62$), this can not be attributed to poor cell spreading because most of the cells were spindled at this time-point. Needless to say, the matrix cannot be compacted when the cells are predominantly rounded. By day 7 there was a good correlation between compaction and modulus ($R^2 = 0.94$), which points to the importance of matrix compliance in modulating cellular contraction, but still does not preclude the effects of proteases that may be actively reducing the effective modulus of the hydrogel concurrently. Therefore, with regard to construct compaction, the cell spreading is certainly a requirement for contraction, but the matrix stiffness that imposes physical impediments to the restructuring process of the material may be equally important.

Mechanism of cellular remodeling

So far, we have been unable to verify that either matrix modulus or proteolytic pathways dominate the cell morphology response in 3D, despite having materials designed to pseudo-independently control proteolytic sensitivity, biological activity, and matrix stiffness. It is assumed that the cellular remodeling of the PF matrix is mediated by a combination of physical matrix remodeling and biochemical matrix remod-

eling. In this context, physical matrix remodeling included deformations of the matrix caused by expansion or contraction exerted by the cells, whereas biochemical matrix remodeling included structural modifications to the material due to the production of matrix degrading enzymes or matrix building proteins. We propose that locally expressed proteases can readily cleave the fibrinogen backbone to alter the mechanics of the matrix, facilitate lamellipodia protrusion, and advance macroscopic construct remodeling.

To verify this hypothesis, we sought a way of visualizing the very first remodeling event expressed by the rounded cells within the hydrogel matrix. To do this, inert polystyrene beads (2 μm) were dispersed with the SMCs into the hydrogel during casting, and visualization of bead displacement was accomplished using time-lapse microscopy. In the Supplementary Material, Video 2 data, it appeared that the rounded cells initially protrude with lamellipodia into the materials without deforming their surrounding matrix. Fig. 7 shows the typical time-course of cellular events after SMC encapsulation, including spreading, contraction, and migration. In Fig. 7 *A* an individual cell is seen extending with lamellipodia whereas the superimposed displacement vectors show negligible bead translation during the initial 6 h. After 12 h, the cellular extensions exert tractional forces causing the matrix to contract toward the cell body. In the very complaint materials (11 Pa modulus), the cell exerts traction that caused very large deformations of the materials after 24 h (Fig. 7 *B*). By day 3, the encapsulated cells migrate toward each other and become interconnected, working together to compact the matrix. Spontaneous disruption of the interconnections between the cells caused viscoelastic recoil of the material (Fig. 7 *C*). Based on these observations, we can speculate that cells proteolytically tunnel through the matrix and form matrix contacts that help to facilitate their contractile behavior. The initial spreading is most likely mediated by proteolysis, whereas the contraction forces are impeded by the matrix stiffness. Once cells interconnect into networks, they can exert traction on the entire construct, resulting in macroscopic compaction (Fig. 6).

The biochemical matrix remodeling associated with cellular activity in the PF hydrogel included the production of structural proteins such as collagen, as well as the secretion of MMPs. The presence of type I collagen in the constructs was examined using immunofluorescence staining of 3 day constructs. The staining showed diffuse and unorganized collagen around the spindled SMCs (Fig. 8 *A*). It was difficult to ascertain from the staining results if the newly synthesized collagen contributed to the structural characteristics of the matrix. To definitively associate between matrix proteases and cellular remodeling, we screened the proteolytic profile of SMC-seeded PF hydrogels using SDS-PAGE gelatin zymography (not shown). Western blotting was used to confirm

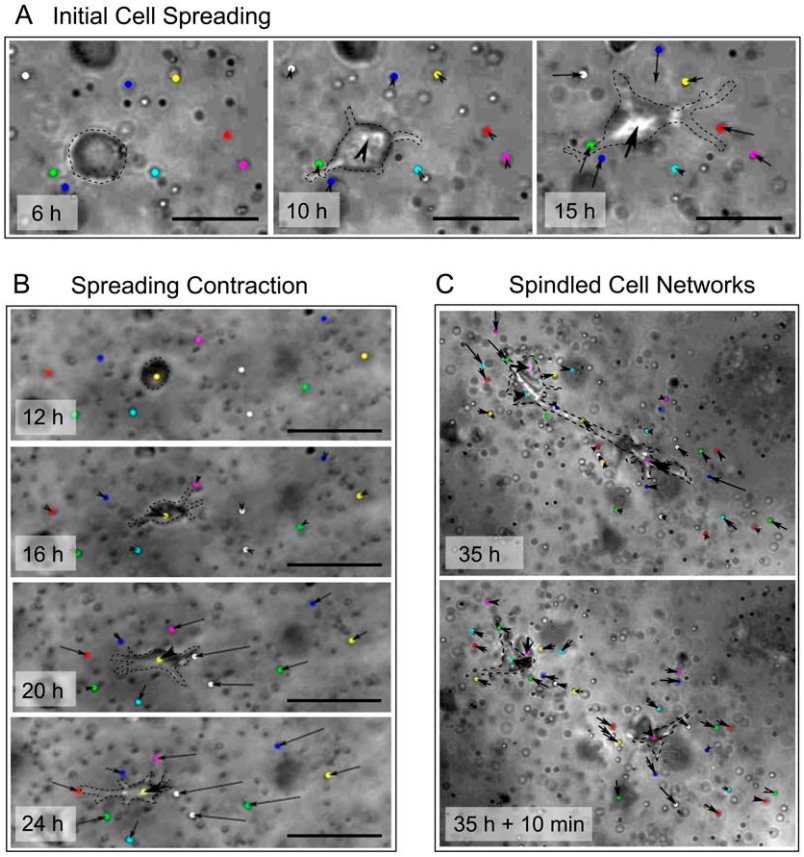

FIGURE 7 The SMCs remodel the PF hydrogel matrix in 3D culture through initial spreading followed by tractional force generation and contraction. The contraction by SMCs was quantified by imaging the cells together with 2-μm beads in sequential image frames and measuring the bead displacement vectors of individual beads surrounding the cells between the time increments (*arrows*). The interaction between cells and the PF matrix was characterized by the magnitude and direction of the bead displacement vectors. (*A*) During the initial 10 h of cells spreading, the cells first extend in the PF matrix without displacing the surrounding beads and then cause radially inward bead displacement (signifying matrix contraction) after 15 h (Supplementary Material, Video 2). (*B*) After 20 h, the cells caused extensive matrix contraction as indicated by the large inward radial bead displacements. (*C*) Eventually, the cells interconnected and produced macroscopic contraction of the PF matrix; when two cells disconnected spontaneously, the PF matrix exhibits viscoelastic recoil. The representative images were of constructs made from PF10 (6 mg/ml).

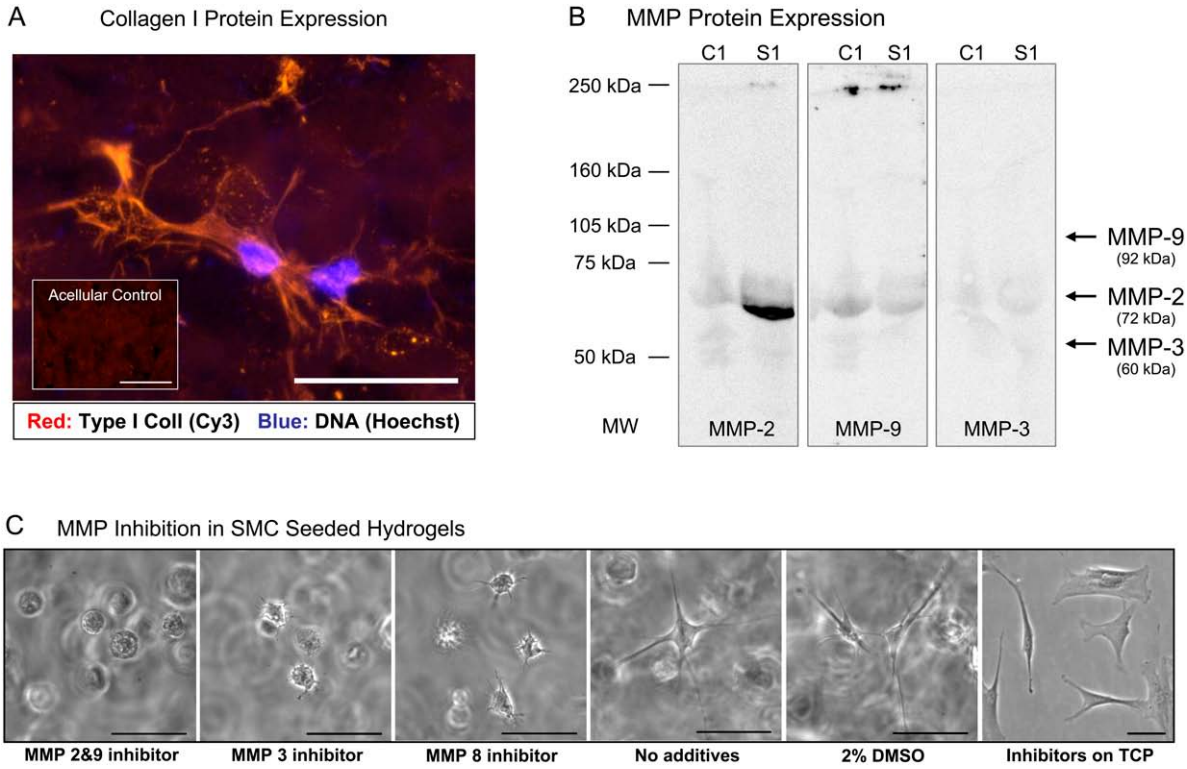

FIGURE 8 SMC remodeling is dependent on protein and protease expression. (*A*) SMCs produce type-I collagen after 3 days in culture (shown: PF10, 6 mg/ml). (*B*) Western blotting detects levels of MMP-2 but not MMP-9 and MMP-3 in the SMC-seeded PF hydrogels after 3 days in culture (s1, sample, c1, acellular controls). (*C*) Selective inhibition of matrix metalloproteinases (MMPs) in SMC-seeded hydrogel constructs alters the morphology of the cells. MMP inhibitors were used to investigate the significance of proteases in the 3D cell spreading process after 2 days in culture. SMCs were cultured in highly compliant materials made from PF10 (6 mg/ml) in the presence of various MMP inhibitors including: MMP 2/9 inhibitor (0.6 mM), MMP 3 inhibitor (0.3 mM), and MMP 8 inhibitor (0.1 mM). Three controls were used in the experiment including: SMCs encapsulated without inhibitors; SMCs encapsulated in 2% DMSO (similar to the DMSO content in the inhibitor solution); and SMCs cultured on tissue culture plastic (TCP) with MMP 2/9 inhibitor (0.6 mM). Scale bars = 50 μm.

the presence of one particular protease in the 3D culture homogenates: MMP-2 (Fig. 8 *B*). Although MMP-3 and MMP-9 were not detected by Western blotting, MMP inhibitors for MMP-2/MMP-9, MMP-3, and MMP-8 each affected the SMC morphology in the 3D matrix when compare with the spindled morphology of control samples (Fig. 8). The fact that MMP-3 was undetected whereas inhibitor for MMP-3 affected SMC morphology underscores the need to expand on the proteolytic inhibition studies in future experiments. Nevertheless, the MMP inhibition data points to the necessity of proteolysis for the expression of spindled cell morphology in all the PF materials, irrespective of their stiffness and proteolytic sensitivity. The MMP inhibitors did not alter the SMC viability or 2-D SMC morphology on tissue culture polystyrene (TCP), even though the concentrations of protease inhibitors that were used were several orders of magnitude higher than their IC_{50} values (12).

Matrix modulus versus proteolysis

The general hypothesis that matrix modulus dominates the cell morphology response in 3D has been difficult to fully validate, despite having materials designed to pseudo-independently control proteolytic sensitivity and matrix modulus. In this regard, one of the drawbacks in this approach was that altering the modulus of the PF hydrogel also altered the proteolytic resistance of the material to some extent. Nevertheless, there were a number of findings that recognized the relative importance of matrix modulus in regulating cellular remodeling. For example, at the onset of cell spreading, the cells seem to rely on proteolysis when extending lamellipodia into the dense hydrogel environment as evidenced by the lack of cellular extension in the MMP inhibition studies. Furthermore, during the initial spreading events, there did not appear to be expansion of the materials immediately surrounding the cells, based on displacement vectors of microscopic beads near the cellular lamellipodia. Instead, cells appeared to proteolytically tunnel in the dense matrix until they formed lamellipodia that were capable of large matrix contraction. Once the cells reached a spindled morphology, macroscopic contraction of the constructs was facilitated by tractional forces and physical resistance to this contraction was imposed by the stiffness of the impeding matrix. A direct link between the macroscopic construct remodeling and the

matrix modulus certainly does not undermine the role of locally secreted cellular proteases that may progressively reduce the effective modulus of the materials. Although more investigation is required to fully validate this hypothesis, we show that the interconnection between matrix modulus and proteolytic resistance may be partly uncoupled to provide more insight into how cells interpret their physical ECM environment.

CONCLUSIONS

We conclude that SMC remodeling of an amorphous hydrogel ECM analog was highly influenced by the material's modulus as well as by the proteolytic resistance of the matrix. Initially, the cells use proteolysis to express their spindled morphology within the dense hydrogel. Once the encapsulated cells obtained a spindled morphology, they exert tractional forces on the matrix to physically contract the hydrogel. The extent of cellular compaction was dependent on the matrix stiffness. The cellular remodeling associated with the compaction of the construct was also accompanied by the production of type-I collagen and ECM proteases. These results support the scientific view that cellular remodeling can be precisely controlled through matrix compliance. Beyond the morphological changes espoused by alterations to the physical environment, cell genotype and phenotype may similarly be manipulated by slight changes to matrix compliance, and this ability to quantitatively evaluate structure/function relationships in 3D tissue morphogenesis can serve as a scientific platform for discovery of new inductive pathways in tissue disease and regeneration.

SUPPLEMENTARY MATERIAL

To view all of the supplemental files associated with this article, visit www.biophysj.org.

Supported by grant 1140/04 from the Israel Science Foundation.

REFERENCES

1. Rehfeldt, F., A. J. Engler, A. Eckhardt, F. Ahmed, and D. E. Discher. 2007. Cell responses to the mechanochemical microenvironment-Implications for regenerative medicine and drug delivery. *Adv. Drug Deliv. Rev.* 59:1329–1339.
2. Pedersen, J. A., and M. A. Swartz. 2005. Mechanobiology in the third dimension. *Ann. Biomed. Eng.* 33:1469–1490.
3. Reddi, A. H. 1998. Role of morphogenetic proteins in skeletal tissue engineering and regeneration. *Nat. Biotechnol.* 16:247–252.
4. Bershadsky, A. D., N. Q. Balaban, and B. Geiger. 2003. Adhesion-dependent cell mechanosensitivity. *Annu. Rev. Cell Dev. Biol.* 19:677–695.
5. Drury, J. L., and D. J. Mooney. 2003. Hydrogels for tissue engineering: scaffold design variables and applications. *Biomaterials.* 24:4337–4351.
6. Shin, H., S. Jo, and A. G. Mikos. 2003. Biomimetic materials for tissue engineering. *Biomaterials.* 24:4353–4364.
7. Friedl, P., and E. B. Brocker. 2000. The biology of cell locomotion within three-dimensional extracellular matrix. *Cell. Mol. Life Sci.* 57:41–64.
8. Zaman, M. H., P. Matsudaira, and D. A. Lauffenburger. 2007. Understanding effects of matrix protease and matrix organization on directional persistence and translational speed in three-dimensional cell migration. *Ann. Biomed. Eng.* 35:91–100.
9. Arora, P. D., N. Narani, and C. A. McCulloch. 1999. The compliance of collagen gels regulates transforming growth factor-beta induction of alpha-smooth muscle actin in fibroblasts. *Am. J. Pathol.* 154:871–882.
10. Friedl, P., K. S. Zanker, and E. B. Brocker. 1998. Cell migration strategies in 3D extracellular matrix: differences in morphology, cell matrix interactions, and integrin function. *Microsc. Res. Tech.* 43: 369–378.
11. Zaman, M. H., L. M. Trapani, A. L. Sieminski, Mackellar, H. Gong, R. D. Kamm, A. Wells, D. A. Lauffenburger, and P. Matsudaira. 2006. Migration of tumor cells in 3D matrices is governed by matrix stiffness along with cell-matrix adhesion and proteolysis. *Proc. Natl. Acad. Sci. USA.* 103:10889–10894.
12. Wolf, K., I. Mazo, H. Leung, K. Engelke, U. H. von Andrian, E. I. Deryugina, A. Y. Strongin, E. B. Brocker, and P. Friedl. 2003. Compensation mechanism in tumor cell migration: mesenchymal-amoeboid transition after blocking of pericellular proteolysis. *J. Cell Biol.* 160:267–277.
13. Friess, W. 1998. Collagen–biomaterial for drug delivery. *Eur. J. Pharm. Biopharm.* 45:113–136.
14. Shapira-Schweitzer, K., and D. Seliktar. 2007. Matrix stiffness affects spontaneous contraction of cardiomyocytes cultured within a PEGylated fibrinogen biomaterial. *Acta Biomater.* 3:33–41.
15. Khatiwala, C. B., S. R. Peyton, and A. J. Putnam. 2006. Intrinsic mechanical properties of the extracellular matrix affect the behavior of pre-osteoblastic MC3T3–E1 cells. *Am. J. Physiol. Cell Physiol.* 290:C1640–C1650.
16. Engler, A. J., S. Sen, H. L. Sweeney, and D. E. Discher. 2006. Matrix elasticity directs stem cell lineage specification. *Cell.* 126:677–689.
17. Pelham, R. J., Jr., and Y. Wang. 1997. Cell locomotion and focal adhesions are regulated by substrate flexibility. *Proc. Natl. Acad. Sci. USA.* 94:13661–13665.
18. McDaniel, D. P., G. A. Shaw, J. T. Elliott, K. Bhadriraju, C. Meuse, K. H. Chung, and A. L. Plant. 2007. The stiffness of collagen fibrils influences vascular smooth muscle cell phenotype. *Biophys. J.* 92:1759–1769.
19. Engler, A., L. Bacakova, C. Newman, A. Hategan, M. Griffin, and D. Discher. 2004. Substrate compliance versus ligand density in cell on gel responses. *Biophys. J.* 86:617–628.
20. Pelham, R. J., Jr., and Y. L. Wang. 1998. Cell locomotion and focal adhesions are regulated by the mechanical properties of the substrate. *Biol. Bull.* 194:348–349 (discussion 349–50).
21. Yeung, T., P. C. Georges, L. A. Flanagan, B. Marg, M. Ortiz, M. Funaki, N. Zahir, W. Ming, V. Weaver, and P. A. Janmey. 2005. Effects of substrate stiffness on cell morphology, cytoskeletal structure, and adhesion. *Cell Motil. Cytoskeleton.* 60:24–34.
22. Peyton, S. R., C. B. Raub, V. P. Keschrumrus, and A. J. Putnam. 2006. The use of poly(ethylene glycol) hydrogels to investigate the impact of ECM chemistry and mechanics on smooth muscle cells. *Biomaterials.* 27:4881–4893.
23. Peyton, S. R., and A. J. Putnam. 2005. Extracellular matrix rigidity governs smooth muscle cell motility in a biphasic fashion. *J. Cell. Physiol.* 204:198–209.
24. Ghosh, K., Z. Pan, E. Guan, S. Ge, Y. Liu, T. Nakamura, X. D. Ren, M. Rafailovich, and R. A. Clark. 2007. Cell adaptation to a physiologically relevant ECM mimic with different viscoelastic properties. *Biomaterials.* 28:671–679.
25. Edelman, D. B., and E. W. Keefer. 2005. A cultural renaissance: in vitro cell biology embraces three-dimensional context. *Exp. Neurol.* 192:1–6.
26. Cukierman, E., R. Pankov, D. R. Stevens, and K. M. Yamada. 2001. Taking cell-matrix adhesions to the third dimension. *Science.* 294:1708–1712.
27. Abbott, A. 2003. Cell culture: biology's new dimension. *Nature.* 424: 870–872.
28. Almany, L., and D. Seliktar. 2005. Biosynthetic hydrogel scaffolds made from fibrinogen and polyethylene glycol for 3D cell cultures. *Biomaterials.* 26:2467–2477.

29. Gonen-Wadmany, M., L. Oss-Ronen, and D. Seliktar. 2007. Protein-polymer conjugates for forming photopolymerizable biomimetic hydrogels for tissue engineering. *Biomaterials*. 28:3876–3886.

30. Seliktar, D. 2005. Extracellular stimulation in tissue engineering. *Ann. N. Y. Acad. Sci.* 1047:386–394.

31. Dikovsky, D., H. Bianco-Peled, and D. Seliktar. 2006. The effect of structural alterations of PEG-fibrinogen hydrogel scaffolds on 3D cellular morphology and cellular migration. *Biomaterials*. 27:1496–1506.

32. Halstenberg, S., A. Panitch, S. Rizzi, H. Hall, and J. A. Hubbell. 2002. Biologically engineered protein-graft-poly(ethylene glycol) hydrogels: a cell adhesive and plasmin-degradable biosynthetic material for tissue repair. *Biomacromolecules*. 3:710–723.

33. Peled, E., J. Boss, J. Bejar, C. Zinman, and D. Seliktar. 2007. A novel poly(ethylene glycol)-fibrinogen hydrogel for tibial segmental defect repair in a rat model. *J. Biomed. Mater. Res. A*. 80:874–884.

34. Thevenaz, P., U. E. Ruttimann, and M. Unser. 1998. A pyramid approach to subpixel registration based on intensity. *IEEE Trans. Image Process*. 7:27–41.

35. Raeber, G. P., M. P. Lutolf, and J. A. Hubbell. 2005. Molecularly engineered PEG hydrogels: a novel model system for proteolytically mediated cell migration. *Biophys. J.* 89:1374–1388.

36. Raeber, G. P., M. P. Lutolf, and J. A. Hubbell. 2007. Mechanisms of 3D migration and matrix remodeling of fibroblasts within artificial ECMs. *Acta Biomater*. 3:615–629.

37. Elbert, D. L., and J. A. Hubbell. 2001. Conjugate addition reactions combined with free-radical cross-linking for the design of materials for tissue engineering. *Biomacromolecules*. 2:430–441.

38. Krsko, P., and M. Libera. 2005. Biointeractive hydrogels. *Mater. Today*. 8:36–44.

39. Veronese, F. M., and G. Pasut. 2005. PEGylation, successful approach to drug delivery. *Drug Discov. Today*. 10:1451–1458.

40. Bailon, P., and W. Berthold. 1998. Polyethylene glycol-conjugated pharmaceutical proteins. *Pharm. Sci. Technol. Today*. 1:352–356.

41. Boulter, E., D. Grall, S. Cagnol, and E. Van Obberghen-Schilling. 2006. Regulation of cell-matrix adhesion dynamics and Rac-1 by integrin linked kinase. *FASEB J*. 20:1489–1491.